Nexus
Research Article

Realizing optimal radiative cooling walls in building-energy nexus via asymmetric emissivity

Qilong Cheng, Sebastian Gomez, Guanzhong Hu, Albatool Abaalkhail, Jazmyn E. Beasley, Peter Zhang, Yuan Xu, Xiaohan Chen, Steven Tian, Jyotirmoy Mandal, Aaswath P. Raman, Nanfang Yu, and Yuan Yang
*Correspondence: jm3136@princeton.edu (J.M.); aaswath@ucla.edu (A.P.R.); ny2214@columbia.edu (N.Y.); yy2664@columbia.edu (Y.Y.)

IN BRIEF

To address overheating issues and reduce cooling energy consumption in buildings, an innovative zigzag wall was implemented to passively achieve optimal radiative cooling effect. Leveraging its asymmetric emissivity design, the wall effectively reflects incoming terrestrial radiation while emitting infrared radiation to outer space. In field tests conducted during summer, this design led to a temperature drop of 2.3°C on average, with its peak at 3.1°C when exposed to hot ground surfaces. The energy impact of this wall design in various application scenarios was thoroughly evaluated. This study provides a practical and accessible solution to efficient thermal management in the building-energy nexus.

Nexus
Research Article

Realizing optimal radiative cooling walls in building-energy nexus via asymmetric emissivity

Qilong Cheng,[1] Sebastian Gomez,[1] Guanzhong Hu,[2] Albatool Abaalkhail,[1] Jazmyn E. Beasley,[2] Peter Zhang,[3] Yuan Xu,[1] Xiaohan Chen,[1] Steven Tian,[2] Jyotirmoy Mandal,[4,5,*] Aaswath P. Raman,[4,*] Nanfang Yu,[1,*] and Yuan Yang[1,6,*]
[1]Department of Applied Physics and Applied Mathematics, Columbia University, New York, NY 10027, USA
[2]Department of Mechanical Engineering, Columbia University, New York, NY 10027, USA
[3]Henry M. Gunn High School, Palo Alto, CA 94306, USA
[4]Department of Materials Science and Engineering, University of California, Los Angeles, Los Angeles, CA 90095, USA
[5]Department of Civil and Environmental Engineering, Princeton University, Princeton, NJ 08544, USA
[6]Lead contact
*Correspondence: jm3136@princeton.edu (J.M.); aaswath@ucla.edu (A.P.R.); ny2214@columbia.edu (N.Y.); yy2664@columbia.edu (Y.Y.)
https://doi.org/10.1016/j.ynexs.2024.100028

SUMMARY

With the gradually warming climate, the global cooling demand for buildings is rapidly increasing. Radiative cooling (RC) has been an attractive electricity-free approach to reducing the energy consumption of buildings. Current RC strategies focus on roofs; however, limited attention has been paid to vertical walls. Here, we report a zigzag-based structural design with asymmetric emissivity to realize optimal RC walls. Such asymmetry leads to a daily average temperature drop of 2.3°C compared to conventional walls coated with RC materials. When the ground is at ~56°C, the temperature drop reaches 3.1°C, corresponding to a relative cooling power of 67 W m^{-2} compared to the control wall. Moreover, the energy impact of this zigzag wall in diverse climate conditions is analyzed based on building-scale simulations. Current limitations and future improvement directions are also discussed. This zigzag RC wall provides a new passive solution to energy-efficient buildings.

INTRODUCTION

Buildings consume ~40% of global energy and account for ~36% of CO_2 emissions,[1] and cooling constitutes ~20% of energy consumption in buildings.[2] The cooling demand keeps rising due to the gradually warming climate. Therefore, efficient cooling methods are critical to reducing energy consumption and associated CO_2 emission in the building-energy nexus and expediting the transition to a carbon-neutral society. Recently, radiative cooling (RC) emerged as an electricity-free approach for cooling by reflecting sunlight (wavelengths [λ] ~0.3–2.5 μm) and emitting long-wave infrared radiation (IR) through an atmospheric transparency window (ATW: λ ~8–13 μm) to the cold outer space. RC has drawn increasing attention in the last 10 years due to advances in materials with both high solar reflectance (R_{solar} > 0.95) and high emittance in ATW (ε_{ATW} > 0.95), such as photonic structures,[3,4] polymers,[5–8] metamaterials,[9,10] cooling wood,[11] and composites.[12–15] With their tailored divergent optical properties at different wavelengths (UV, visible, near-IR, ATW), RC is promising in application in roofs,[4,16,17] windows,[18,19] heat exchangers,[20,21] and greenhouses,[22] which serve as a passive alternative to reduce energy consumption and lower a carbon footprint.

While various RC designs have been successfully applied to rooftops that occupy limited areal portion in building envelopes, they are not ideal for walls, which cover the major portion of building envelopes. The main challenge for RC walls is that they face both cold space and hot ground. Thus, their radiative heat transfer with the ground needs to be taken into consideration. The ground usually has a higher surface temperature than the ambient air (dry bulb) due to daytime solar heating and heat preservation,[23] which can reach ~60°C–70°C at peak.[24] Also, ground materials (e.g., concrete, brick, asphalt) typically have high thermal emissivity ε > 0.9,[25] resulting in significant thermal radiation to the walls (e.g., ~90 W m^{-2} at 60°C and ε_{ground} = 0.95). Consequently, conventional RC designs with a high emissivity will receive considerable heat from the ground, and thus are not effective for RC walls (Figure 1A).

RC walls have gained limited attention so far, and current designs have limitations. An ATW selective emitter was reported to reflect the terrestrial thermal radiation outside of this wavelength band and keep the RC within the band,[26] but the vertical surface still suffers strong radiation in the ATW from the ground, which accounts for ~40% of the total thermal radiation at 40°C–60°C. Low-emissivity (low-E) films have been developed for building walls to reject radiation from the hot ambient environment,[27] but the heat loss to the cold space through the ATW is also abandoned. An angle-selective emitter was recently proposed to achieve energy savings by outdoor RC at building walls,[28] but its microstructure requires extensive manufacturing efforts.

Standing at the crossroads of building engineering, optics, and heat transfer, we leverage geometrical optics and propose a zigzag-based structural wall design with asymmetric emissivity to provide a more practical and accessible solution to efficient thermal management in the building-energy nexus, which is easier to implement in a scalable fashion. The zigzag design consists of an IR emissive surface facing the sky and an IR reflective surface facing the ground (emissive/reflective zigzag [ERZ] wall), which maximizes the wall's net RC power. In our design (Figure 1B), the IR emissive surface that faces the sky can still radiate the thermal emission through the ATW, achieving RC. In contrast, the IR reflective surface such as metalized film faces the hot ground and reflects the IR from the ground, which decreases the heat gain. The additional zigzag structure basically does not affect the thermal resistance of the building walls (Figure S2D).

To validate the effectiveness of this design, spectral irradiances of net heat gain from the ground and the net heat loss to the space were simulated for a conventional flat emissive wall (high-E wall, Figure 1C) and an ERZ wall (Figure 1D), respectively (see supplemental information, section 1). The high-E wall is assumed to be an ideal broadband emitter, and the ERZ wall is composed of an ideal emitter and an ideal reflector. As shown in Figures 1C and 1D, at a ground surface temperature of 60°C and a wall temperature of 30°C, the high-E wall gains 89.7 W m^{-2} from the hot ground, while the ERZ wall only receives 15.1 W m^{-2}. Such a large reduction arises from the larger view factor (0.75) from the reflective bottom surface of the ERZ wall to the ground, compared to 0.5 for the high-E wall. On the other side, the high-E wall loses 40.9 W m^{-2} heat to the space, but the ERZ wall with a smaller emissive area loses a slightly higher amount of 42.2 W m^{-2}. This is due to the high view factor (0.93) of the top emissive surface to the sky in the ERZ wall, compared to 0.5 for the flat high-E wall, and the fact that the sky emittance is lower near the zenith and higher near the horizon.[29]

Consequently, the ERZ wall's effective angular emissivity is ~0.91 facing the sky, but only ~0.08 facing the ground, showing a significant angular asymmetry (Figure 1F). In addition, an ideal low-E wall has a net heat exchange of 0 W m^{-2} because its zero emissivity does not

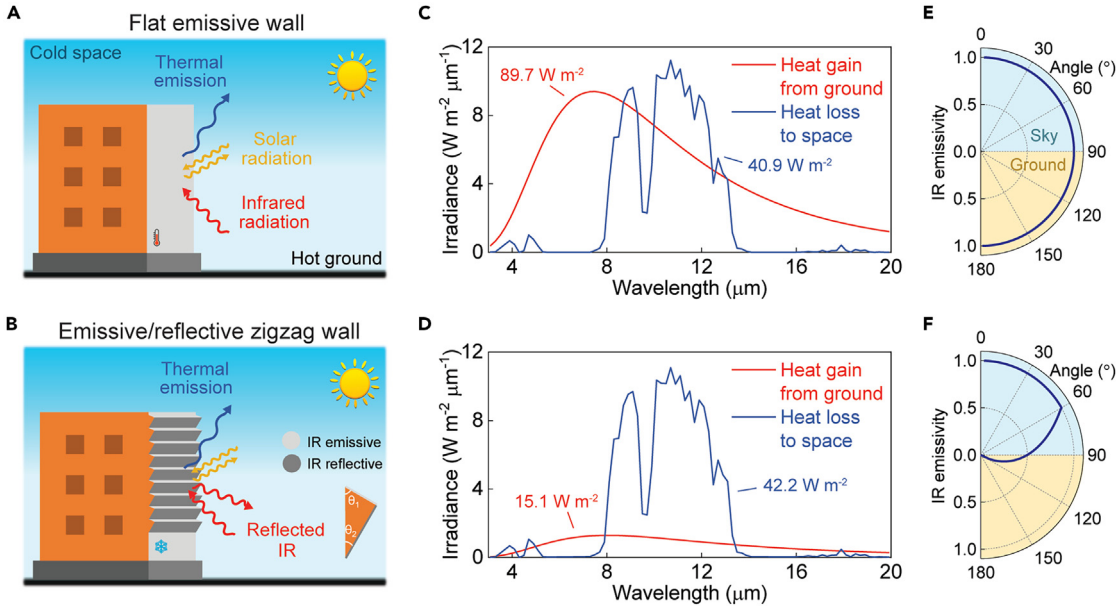

Figure 1. Conceptual illustration of ERZ walls

(A) Schematic of a conventional flat emissive wall ($\lambda \geq 2.5$ μm: $\varepsilon = 1$), showing mechanisms of its heat transfer with the surroundings.

(B) Schematic of an ERZ wall. Top surface: an ideal broadband emitter ($\lambda \geq 2.5$ μm: $\varepsilon_{top} = 1$). Bottom surface: an ideal broadband reflector ($\lambda \geq 2.5$ μm: $\varepsilon_{bottom} = 0$). The wall can reflect the IR from the hot ground while maintaining the thermal emission toward the cold space, achieving further building cooling than flat walls coated with RC materials.

(C and D) Simulated net heat gain from the ground (60°C, heat exchange between the ground and the wall) and net heat loss to the space (heat exchange between the sky and the wall) for the flat high-E wall (C) and the ERZ wall (D). The wall surfaces and the ambient air are set at 30°C. The powers are normalized by the nominal footprint wall area. The ERZ wall features a much lower heat gain (16.8%) and a slightly higher heat loss (103.2%) compared to the flat high-E wall.

(E and F) Simulated angular IR emissivity of a flat high-E wall (E) and an ERZ wall (F). The flat high-E wall has a uniformly high emissivity facing the sky or the ground, while the ERZ wall shows a significant angular asymmetry.

In (D) and (F), the ERZ wall has a geometry of $\theta_1 = 60°$, $\theta_2 = 30°$.

allow any radiative heat transfer. Therefore, the ERZ wall with asymmetric emissivity can achieve more significant building cooling than flat walls with either high-E or low-E, and even sub-ambient RC, which is later demonstrated both numerically and experimentally.

RESULTS

Theoretical cooling potential of ERZ walls

Unlike previous RC studies where the only tunable degrees of freedom are optical properties of materials, the zigzag-based structural design further utilizes a new degree of freedom, angular asymmetry, to maximize the cooling performance. This zigzag geometry can be described by two parameters as the critical angle between the vertical direction and the top surface θ_1 or the bottom surface θ_2 (Figure 2A). Moreover, the surface specularity also plays an important role in the cooling performance, since light can bounce between different wall surfaces multiple times (Figures 2B, inset, and 2C).

To understand the effects of the angular asymmetry and maximize the cooling performance, we first investigated the impact of specularity at (top, bottom) surfaces by calculating the relative cooling power P_{cool}, which is defined as the extra cooling power of an ERZ wall in comparison with a flat high-E wall that has the same emissivity as the side facing the sky in the ERZ wall (see supplemental information, section 1). In the (s, s) case, where both the surfaces are specularly reflective, the ERZ wall shows the largest P_{cool} (Figure 2B). Such results are also consistent with our qualitative analysis (Figure 2C) and experimental data (Figure S10) that specular opaque surfaces should result in less solar absorption and less IR absorption than diffuse ones, since some portion of the radiation is reflected away without bouncing among zigzags. Similar results are also observed in other (θ_1, θ_2) combinations (Figure S5). Therefore, both surfaces are set at a specularity of 1 in the following analysis.

The relative cooling powers P_{cool} at an extensive range of (θ_1, θ_2) combinations were further surveyed for both day (Figure 2D) and night (Figure 2E). In daytime, when the solar zenith angle is 30°, the relative cooling power $P_{cool} > 70$ W m^{-2} occurs at (45°–60°, 25°–35°). At night, the maximum relative cooling power P_{cool} reaches 78.6 W m^{-2} at (90°, 30°), but remains nearly a constant for (60°–90°, 25°–35°) because of almost unchanged thermal emission to the cold space and absence of solar absorption at night. At other solar zenith angles, (θ_1, θ_2) of (60°, 30°) also achieves nearly optimal P_{cool} (Figure S3), and their complementary values provide convenience for prototype fabrication.

The relationship between P_{cool} and varying ground surface temperatures shows that the ERZ wall provides a positive P_{cool} when the ground surface temperature exceeds ~35°C and that a higher ground surface temperature induces a larger cooling advantage because more incoming IR is rejected (Figure 2F). From the simulations, we also observe that the ERZ wall's cooling performance slightly deteriorates with increasing solar absorptance (Figure S4). However, this effect is minor and can be reduced by using materials with high R_{solar} over 0.95 (Figure S16). In addition, it should be noted that the dimension of one zigzag period itself does not affect the cooling performance if it is significantly larger than relevant thermal wavelengths below 50 μm (Figure S6), which guarantees convenient fabrication and scalability.

Cooling performance of ERZ walls

To experimentally demonstrate the cooling performance of ERZ walls, we fabricated samples with scalable and low-cost materials as a proof of concept. Aluminized Mylar films were used as the IR reflector facing the hot ground since they have a specularity >0.98 (Figure 3A). Polydimethylsiloxane (PDMS, ~150 μm) coated Mylar films were used as the IR emitter that faces the sky due to high thermal emissivity and the optical transparency of PDMS,[30] which retains a high specularity of ~0.94 (Figure 3B). The reflector and the emitter show nearly identical solar reflectance (~0.87), while their IR emittances (0.08 and 0.94) differ greatly. It is worth noting that thinner PDMS-coated Mylar films are also feasible and can save material costs.

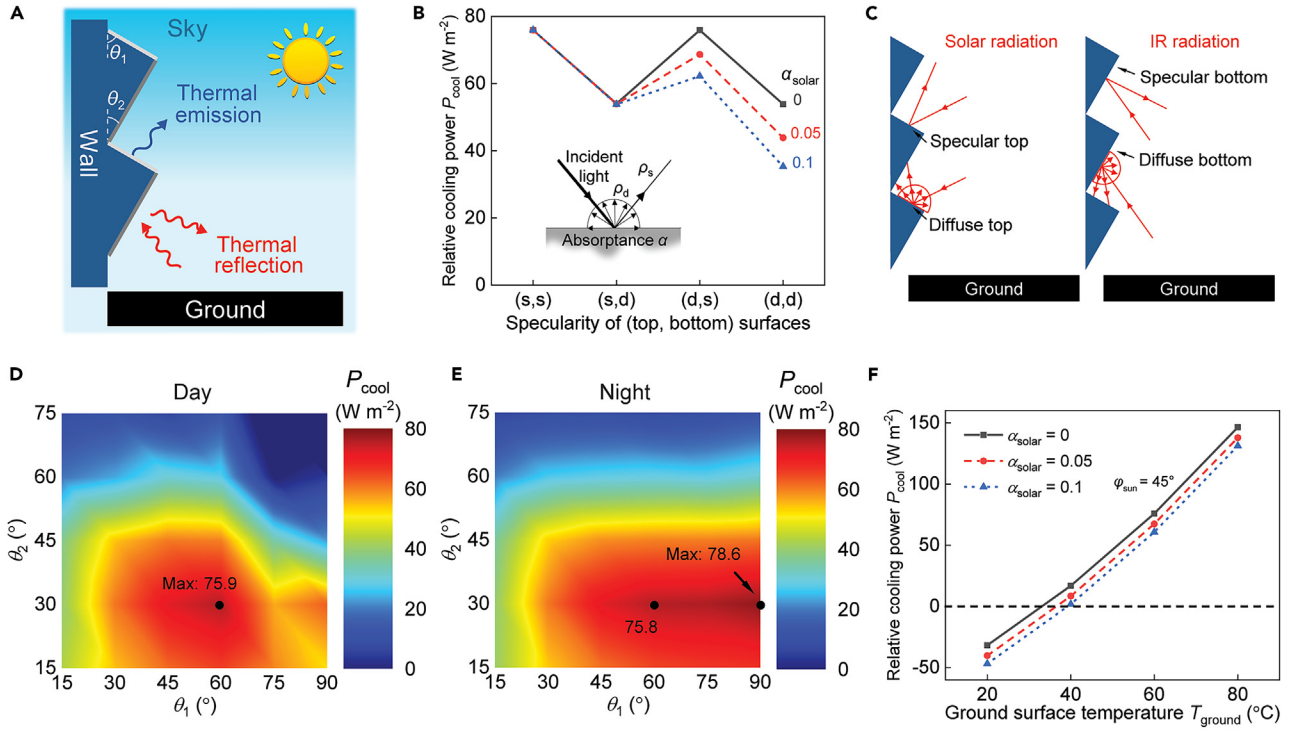

Figure 2. Simulations on cooling performance of ERZ walls

(A) Schematic of the ERZ wall configuration used in the simulations, featuring two critical angles, θ_1 and θ_2.

(B) Simulated relative cooling power P_{cool} as a function of specularity of the two surfaces (s: specularity = 1; d: specularity = 0) and their solar absorptance α_{solar}. To calculate P_{cool}, an energy flux is applied to the back of a wall to keep its exterior at the same temperature as the ambient air, and P_{cool} is the difference of the energy fluxes for the ERZ wall and the high-E wall: $P_{cool} = P_{cool,\ ERZ} - P_{cool,\ high\text{-}E}$ (see Figure S2C). Inset: schematic of diffuse reflectance ρ_d, specular reflectance ρ_s, and absorptance α for an opaque surface. Specularity is defined as $\rho_s/(\rho_s + \rho_d)$.

(C) Schematics showing how specularity reduces solar absorption and IR absorption among zigzags.

(D and E) P_{cool} contours over θ_1 and θ_2 with sunlight present (D) or without sunlight (E). The solar absorptance α_{solar} is set as 0.05 on all wall surfaces. $(\theta_1, \theta_2) = (60°, 30°)$ leads to optimal results.

(F) The relationship between P_{cool} and the ground surface temperature.

In (B) and (D), the solar zenith angle is 30° to represent a typical case for afternoons in the southern United States, while the solar zenith angle is 45° in (F) to show the effect of enhanced solar absorption on the wall from light bouncing. P_{cool} contours at other solar zenith angles of 0°, 60°, and 90° are presented in Figure S3. In (B), (D), and (E), the ground surface temperature is always 60°C.

The reflectors and the emitters were attached on aluminum (Al) parts, which were laminated on the substrate with its back affixed with a thermocouple (TC) and sealed with polystyrene (PS) foam as heat insulation (Figures 3C and 3D). The hollow of the Al parts at the sample lateral surfaces was covered with Al tape. The TC was positioned at the center of the substrate back surface to capture the average temperature of the sample. As the zigzag feature size is in centimeter scale, it is convenient to fabricate such structures by molding in a scalable fashion.

Significant cooling was observed in the ERZ wall prototype compared to each of (1) a flat wall covered only with PDMS/Al/Mylar emitters (high-E wall), (2) a flat wall covered only with Al/Mylar reflectors (low-E wall), and (3) a wall with the same zigzag structure but only PDMS/Al/Mylar emitters (emissive/emissive zigzag [EEZ] wall). In lab tests with a simulated sky made of ice/water mixture and a ground made of cinefoil heated to 60°C (Figure S8), the ERZ wall's temperature rise is 2.9°C, 1.6°C, and 2.8°C lower than that of the high-E wall, the low-E wall, and the EEZ wall, respectively, under simulated day conditions (Figure 3E). During the night, the ERZ wall is 3.0°C, 1.3°C, and 2.8°C cooler than the three controls, respectively. The experimental results also show that the optimal cooling performance is achieved at $\theta_1 = 60°$ under the constraint of $\theta_1 + \theta_2 = 90°$, which agrees well with the simulation results (Figures 2D and 3F). It should be noted that the simulated ice/water sky is not as cold as the real sky, and it has a limited view factor for the wall samples, so the RC to the simulated sky in the lab tests is not as efficient as the real sky. Thus, the lab tests show temperature rise instead of temperature drop, as compared to the ambient temperature.

Following the success in the lab tests, we further demonstrated the advantages of ERZ walls in field tests, which were carried out in summer 2022 in New Jersey (Figures 3G and S12). As shown in Figure 3H, the ERZ wall was always cooler than the control (high-E wall) for a continuous 24 h, where the ground surface temperature ranged from 23°C (07:06 hours) to 56°C (14:29 hours). The ERZ wall was also cooler than the ambient air temperature most of the time (20:00–10:47 hours and 16:35–20:00 hours), except for the hottest period (10:47–16:35 hours), when the ground (>45°C) gave off the strongest thermal radiation, which was absorbed by the top emissive surface after specular reflection at the bottom surface. Nevertheless, the average temperature of the ERZ wall was still 1.2°C lower than the ambient air. Also, another field test shows that the ERZ wall was on average 1.0°C cooler than the low-E wall (Figure S13), demonstrating the advantage of the ERZ wall. The temperature simulation shows consistent results and further confirms that the ERZ wall performs better than the wall with a single valued emissivity, whether high-E or low-E (Figure S15A).

In comparison with the high-E control, the temperature of the ERZ wall was 2.3°C lower on average, and this value reached a peak of 3.1°C between 13:00 and 14:00 hours (Figure 3I). This appears counterintuitive since it indicates that the most pronounced cooling occurred at the hottest time. Such a phenomenon can be explained as that the calculated temperature difference is between the ERZ wall and the flat high-E wall, instead of between the ERZ wall and the ambient, so the high ground surface temperature at 13:00–14:00 hours (>50°C) enlarges the difference of heat absorption at these two walls from the ground, leading to the maximum temperature difference between them. The temperature drop also demonstrates good agreement with the simulation (Figure 3I).

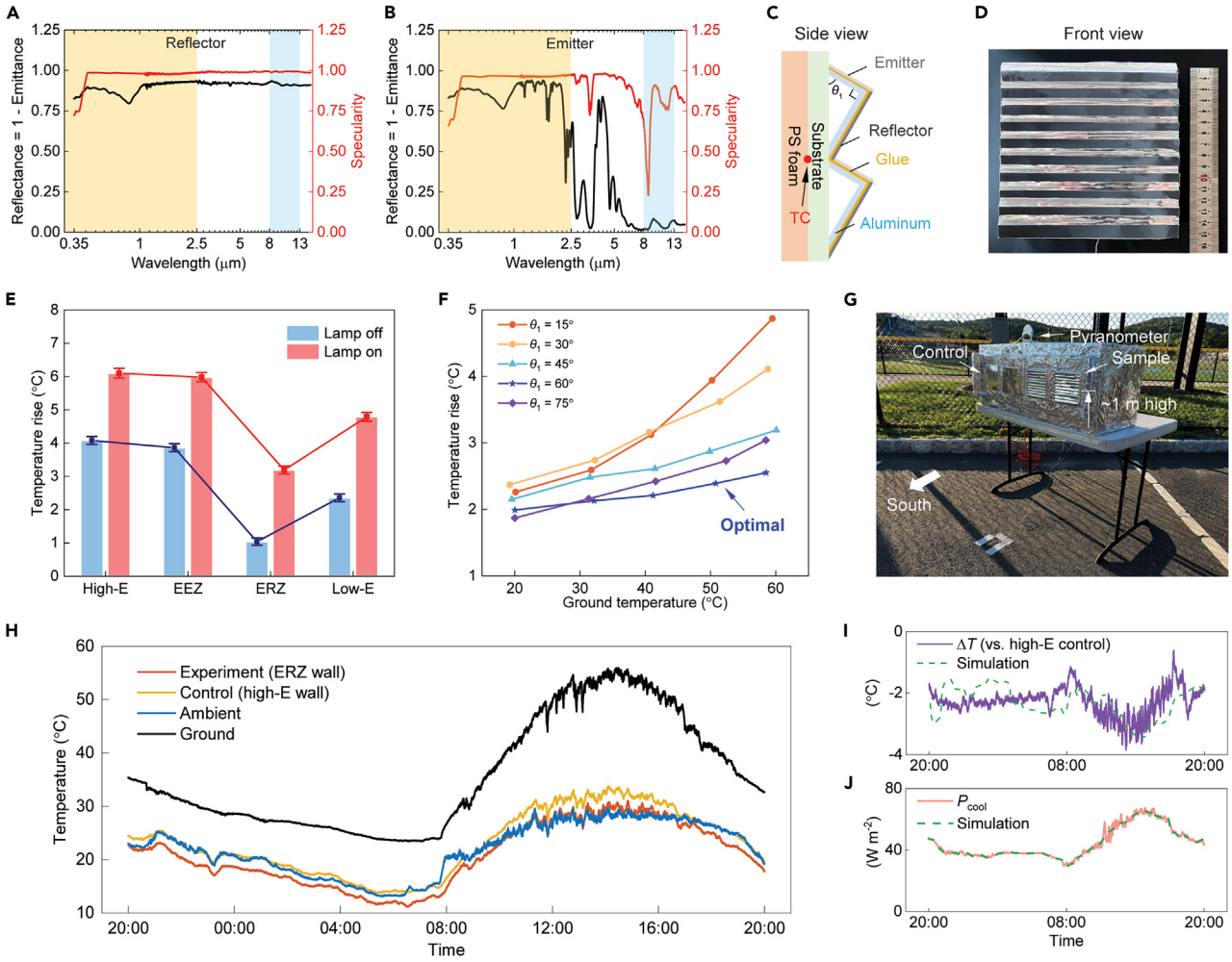

Figure 3. Fabrication of ERZ walls and experiments on its cooling performance

(A and B) Spectral reflectance ($\rho[\lambda] = 1 - \varepsilon[\lambda]$) and specularity of the reflector (A) and the emitter (B), which covers the ERZ wall. They have nearly the same reflectance in the solar spectrum (0.87 for A vs. 0.86 for B) and high specularities in the whole spectrum.

(C) Schematic of the ERZ wall fabrication. The critical angles θ_1 and θ_2 are complementary for simplicity of fabrication.

(D) Front view of the ERZ wall sample. The sample is 15 × 15 cm.

(E) Steady average temperature data of various samples in lab tests ($\theta_1 = \theta_2 = 45°$). The lamp irradiance on the samples is ~81 W m^{-2}.

(F) The dependence of temperature rise on θ_1 at different ground surface temperatures for the ERZ wall. Error bars are <0.15°C.

(G) The experimental setup for field tests in Sparta Township, NJ.

(H) Temperature data over a continuous 24 h. The solar irradiance peaked at ~460 W m^{-2} facing south or ~930 W m^{-2} facing upward (Figure S12C).

(I and J) Temperature drop ΔT (I) and relative cooling power P_{cool} (J) of the ERZ wall as compared to the high-E control.

We further estimate the relative cooling power P_{cool} of the ERZ wall from the temperature data in Figure 3H, which is in the range of 30–67 W m^{-2} in 1 day (Figure 3J, see supplemental information; section 3). Similarly, the P_{cool} shows the same trend as the temperature drop that its peak 67 W m^{-2} appeared at the hottest period of 12:00–15:00 hours, which also coincides with the data in Figures 1C and 1D (heat rejection ~76 W m^{-2}). In addition to the experiments above, we also tested the ERZ wall facing southwest, and the temperature drop reached ~2.6°C (Figure S17), demonstrating that the cooling effect is generic. Moreover, we tested the ERZ walls partially covered by polyethylene (PE) films, which further reduces heat exchange due to air convection but still allows IR to pass. A larger temperature drop of ~4.7°C compared to the high-E wall was achieved (Figure S18), indicating further potential to enhance the cooling performance. In addition to wall samples, a building model with ERZ walls was tested against one with high-E walls or low-E walls, and the corresponding temperature drop was 1.03°C or 0.55°C (Figure S14), stepping closer to the implementation of this ERZ design to actual buildings.

Besides results based on the low-cost PDMS/Al/Mylar surfaces, full-day sub-ambient cooling is achieved by using a silver (Ag)-coated ERZ wall with a higher R_{solar} of 0.95 (Figures 4A and S16). In the continuous 24 h, the Ag ERZ wall was cooler than the high-E control by 2.2°C on average (Figure 4B), and the temperature drop reached 3.2°C at 14:00–15:00 hours. The Ag ERZ wall was also always cooler than the ambient air by 1.4°C on average, and their difference maximized at −6 °C at the first sunshine (Figure 4C). In the hot afternoon (12:00–17:00 hours), the silver ERZ wall was still 0.26°C–1.29°C cooler than the ambient temperature. The experimental data are consistent with the simulation results (Figure S16C), and the simulation again shows that the ERZ wall outperforms the low-E wall. Moreover, a comparison between other approaches for RC walls and this work is provided (see supplemental information, section 5). The ERZ wall presents a more practical design with excellent performance.

DISCUSSION

Effects of thermal insulation

In the aforementioned experimental validation, we used thin polyacrylate walls with a low R value (R = 8.0 × 10^{-3} m^2 K W^{-1}) to align with previous experiments on cooling roofs.[4–6,11] For practical thicker

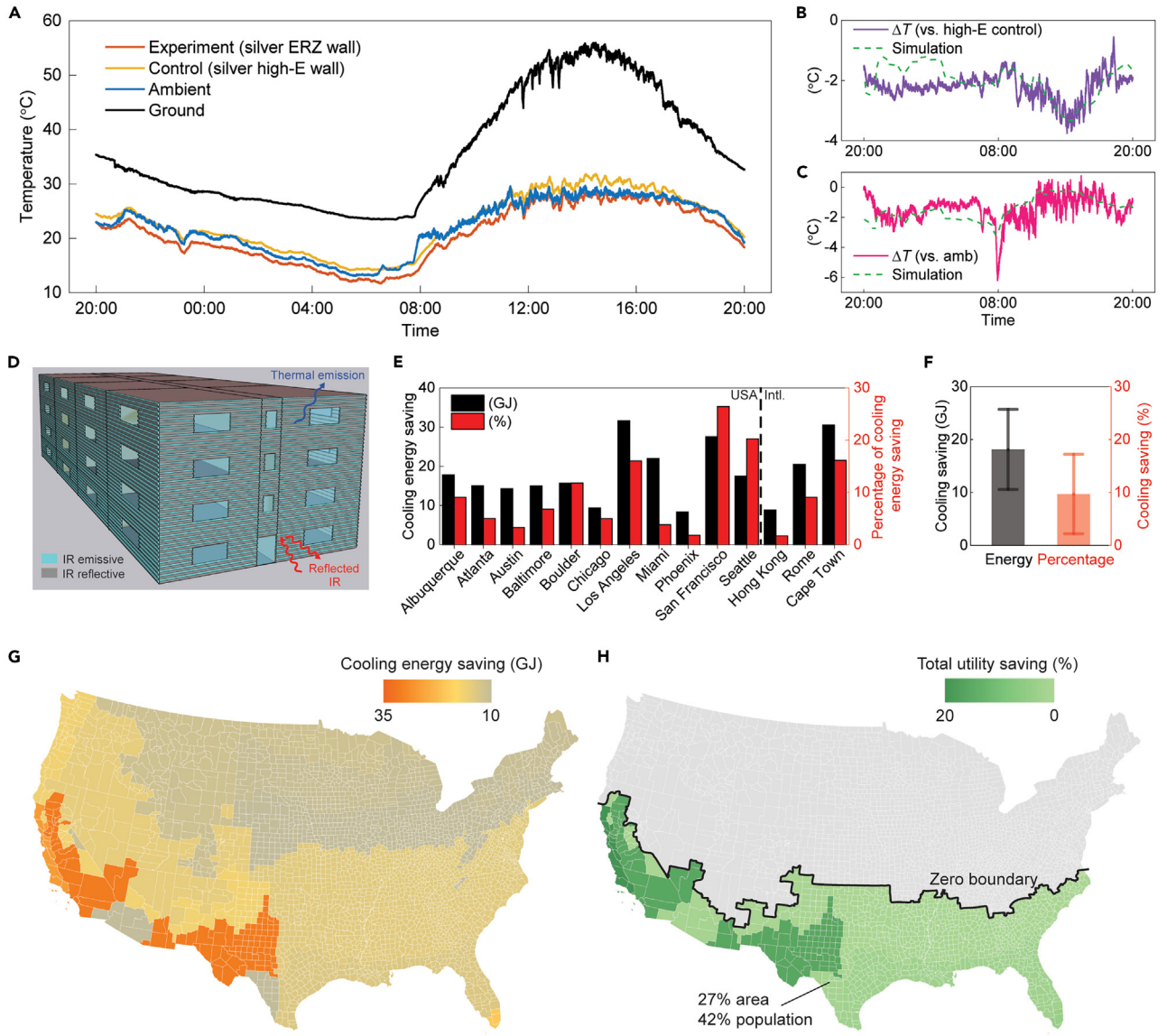

Figure 4. Sub-ambient cooling performance and potential energy savings of ERZ walls

(A) Temperature data of Ag ERZ wall over a continuous 24 h. The samples were measured at the same time as Figure 3H.

(B) Time-dependent temperature drop ΔT between the Ag ERZ wall and the Ag high-E control.

(C) Time-dependent temperature drop between the Ag ERZ wall and the ambient temperature.

(D) The midrise apartment building model used in EnergyPlus simulations, with ERZ walls.

(E) Annual cooling energy savings and percentage of a midrise building with ERZ walls as compared to the same building with high-E walls among 11 cities in the United States and 3 international cities.

(F) Average annual cooling savings and percentage of the 11 cities in the United States together with their SDs.

(G and H) Annual savings maps of cooling energy (G) and total utility (H) of a midrise building with ERZ walls as compared to the same building with high-E walls.

walls, the simulation results (Figure S15B) show that up to the standard thermal insulation (2 m^2 K W^{-1}), there is no significant change in the average $T_{ERZ,\ interior} - T_{high\text{-}E,\ interior}$ (e.g., −2.3°C for R from 8.0 × 10^{-3} m^2 K W^{-1} to 1 m^2 K W^{-1} and −2.2°C for 2 m^2 K W^{-1}). Here, $T_{ERZ,\ interior}$ and $T_{high\text{-}E,\ interior}$ are defined as the temperature at the back of the thermal insulation layer, which corresponds to indoor wall temperature (Figure S15A, inset). When R further increases to 5 m^2 K W^{-1}, the variations in $T_{ERZ,\ interior} - T_{high\text{-}E,\ interior}$ are delayed, and the average of $T_{ERZ,\ interior} - T_{high\text{-}E,\ interior}$ remains at −1.3°C for 5 m^2 K W^{-1}, which is still remarkable.

Energy savings of ERZ walls

To quantify the potential energy savings of ERZ walls at different climate zones, we conducted simulations of energy consumption in buildings using EnergyPlus (see supplemental information, section 4). In the simulations, a midrise apartment building with ERZ walls on all four sides was compared with the same building with flat high-E walls (Figure 4D). The building is a commercial reference defined by the US Department of Energy (DOE).[31] Standard thermal insulation provided by the DOE reference was applied in all simulations. The only input used in the EnergyPlus simulations is the spectra properties of the emissive surface (R_{solar} = 0.86, $\varepsilon_{thermal}$ = 0.95) and the reflective surface (R_{solar} = 0.87, $\varepsilon_{thermal}$ = 0.05), but not near-surface temperature measured in Figure 3H.

In the summer, the ERZ wall can provide annual cooling energy saving of 8–32 GJ or 6.4–24.1 MJ m^{-2} (2%–26%) as compared to the high-E wall for a midrise building in 11 cities in the United States and 3 international cities (Figures 4E and 4F). In particular, Los Angeles, San Francisco, and Cape Town (South Africa) show the largest cooling gain of ∼30 GJ (22.9 MJ m^{-2}), indicating that the ERZ design is best for warm weather.

Similarly, the annual savings map of cooling energy shows that the cooling gain changes from ~32 GJ (24.1 MJ m^{-2}) in the southwest down to ~8 GJ (6.4 MJ m^{-2}) in the north (Figure 4G).

To comprehensively understand the energy impact of ERZ walls, the heating penalty in winter should also be taken into account. For the year-round savings, we chose 16 representative cities in the 16 climate zones in the United States,[32] and mapped the annual energy savings and utility savings there (Figures 4H and S22). The maps demonstrate that for a midrise apartment building, the ERZ wall can provide an annual total energy savings of up to 34 GJ (26.0 MJ m^{-2}; Figure S22C) and ~14% (Figure S22D), which corresponds to an annual total utility savings up to $1,300 (Figure S22E) and ~20% (Figures 4H and S22F) in most of the southern United States. The area where the ERZ wall has net savings accounts for 27% of the land area and 42% of the population (Figure 4H). In these regions, warm summers and mild winters make the cooling utility savings outweigh the heating penalty. In cold regions, the benefit in cooling is overshadowed by the increased heating demand.

Real-world implementation: Application scenarios

The energy savings of ERZ walls are attributed to the reflection of terrestrial thermal radiation and the retention of RC. Thus, the ERZ walls are more applicable in warm regions where the ground surface temperature remains high. Also, the view factor from the wall surface to the ground affects the cooling performance. For example, the ERZ walls are more suitable to be implemented on low-rise buildings than on high-rise buildings because walls at lower heights have a larger view factor to the ground and can reflect more terrestrial radiation.

Similarly, the building walls with adjacent buildings nearby will experience less hot ground surface than those in isolated buildings. Analysis shows that the ERZ wall can still reach attractive cooling performance and energy savings when it is surrounded by adjacent buildings, such as an annual total energy savings of 29.5 GJ (22.5 MJ m^{-2}) in Los Angeles at a building-to-building distance of 10 m (Figure S23). Meanwhile, for buildings with different volume-to-wall-surface ratios (e.g., larger buildings), the ERZ wall still provides effective savings >22 MJ m^{-2} and >9% compared to the conventional high-E wall (Figure S24).

Real-world implementation: Scalable manufacturing, building integration, and cost

The zigzag walls could also be manufactured on a large scale. Using a larger period of zigzag repeating units of 5–50 cm instead of ~1.5 cm in the paper does not compromise optical performance since the geometric dimension is much larger than wavelengths of interest. Such larger structures can be manufactured by using a mold to press metal sheets first, followed by applying high-E coating (e.g., painting or laminating a film) to the side facing the sky, and applying low-E coating (e.g., laminating a reflective film) to the side facing the ground. Regarding current buildings, the manufactured zigzag walls can be mechanically mounted on their exterior surface using threads. In future building designs, wave-like corrugated walls[33] with centimeter-scale corrugation that have already been widely used in building envelopes can be considered, and naturally, the high-E and low-E coatings can be applied on the top and bottom surfaces of corrugations to achieve radiative thermal management. The utilization of corrugated walls validates the feasibility of large-scale implementation of the zigzag walls. The cost of corrugated walls is typically $60/$m^2$, and the current market is around 3 billion dollars globally[33] and is expanding rapidly.

Taking a midrise apartment building in Los Angeles as an example (1,310 m^2 wall area), the additive material cost would be ~$3,000 if Al sheets of 0.3-mm thickness and PDMS of 40-μm thickness are used (see supplemental information, section 7), which is equivalent to $2.3/$m^2$, much lower than commercial corrugated walls. These extra costs can be paid back within 3 years by the utility savings (Figure S22E). In this work, the demonstration of the ERZ design is through the combination of PDMS and Al, but this combination's stability against corrosion and costs needs further examination for practical applications. In addition, there are other promising material strategies and material candidates such as corrosion-resistant and self-cleaning coatings[34] for Al or metal alloy counterparts and transparent radiative coolers (e.g., acrylic based,[35] silica based[36]) as replacements for PDMS.

Real-world implementation: Reducing light pollution and dust accumulation

Although the zigzag design has been proven to be a promising approach for the thermal management of building-energy nexus, there remain some issues that require further research and development. The optimized ERZ walls consist of emitters and reflectors with high specularity. One potential issue of such high specularity is light pollution, but this can be addressed by using a thin layer of visibly opaque but IR-transparent nanoporous PE (nano-PE) as the cover. The diffuse reflection of nano-PE in visible light renders a diffuse appearance, but its high IR specular transmittance >~80% in 8–13 μm at incident angles of 0°–70° indicates that it does not affect the radiative heat transfer between the ERZ walls and the surroundings (Figure S11). Also, the scalable production of nano-PE makes it suitable for such a large-area application in the building envelopes (see supplemental information, section 2). It should be noted, however, that nano-PE and PE films are not widely used as building materials. Their limitations and challenges need to be evaluated further for practical applications. Additionally, the protruded zigzag geometry may induce dust accumulation during operation. This can be addressed by using self-cleaning materials,[37,38] which also require further investigation.

Conclusion

We developed a zigzag-based wall structure with asymmetric emissivity for thermal management in the building-energy nexus. The ERZ wall exhibits better cooling than conventional walls with either high-E or low-E, since it can simultaneously reflect the thermal radiation from the hot ground and remain emissive to the cold space. The cooling performance was confirmed by steady-state simulations, real-world field tests, and EnergyPlus simulations. Such structures can also be fabricated in a scalable fashion by simple molding. Furthermore, the ERZ wall can be combined with state-of-the-art daytime RC materials or responsive RC materials to further enhance the thermal efficiency of building envelopes. Such diverse possibilities make the ERZ wall a viable pathway for smart and sustainable buildings.

EXPERIMENTAL PROCEDURES

Reflector/emitter fabrication

The reflector is a low-cost aluminized Mylar film bought from Amazon.com with a thickness of ~50 μm. The emitter is the Mylar film above coated with PDMS. The PDMS is Dow Corning Sylgard 184 Silicone Elastomer purchased from Krayden. The base and the curing agent were mixed in a 10:1 weight ratio, degassed, drop cast on the reflective Mylar film, and cured under room temperature for 3 days. The cured PDMS thickness is ~150 μm. The reflectors and the emitters were then cut to size by blade for the assembly of the wall samples. Thinner PDMS (e.g., 40 μm thick) can realize almost the same performance and significantly save the material costs (see supplemental information, section 6).

Optical characterization

The total and diffuse reflectances ($\rho_s + \rho_d$, ρ_d) of the reflector, emitter, cinefoil, and white acrylic paint were determined separately in three wavelength bands—0.35–1.1 μm, 1.1–2.5 μm, and 2.5–15.4 μm. In the first band, measurements were taken with an integrating sphere (Thorlabs IS200) and a high-power supercontinuum laser (SuperK Extreme, NKT Photonics) coupled with a tunable band-pass filter (Fianium LLTF contrast). The second and the third spectra (near-IR and mid-IR) were measured using a Fourier transform infrared spectrometer (Bruker Vertex 70v) and a gold (Au) integrating sphere (Labsphere 4P-GPS-020-SL) along with a mercury cadmium telluride detector. A diffuse reflector, 1.66 mm thick porous poly(vinylidene fluoride-hexafluoropropylene),[5] was used as a reference for 0.35–1.1 μm, and Au-coated silicon was used as a reference for 1.1–2.5 μm and 2.5–15.4 μm. The total and diffuse reflectances ($\rho_s + \rho_d$ and ρ_d) were measured with angles of incidence of 30° and 0°, respectively. The three reflectance spectra were patched together. The specularity, solar reflectance R_{solar}, and

emittance ε were calculated using the following equations. $I_{AM\ 1.5G}$ is air mass 1.5G solar spectrum, and I_{bb} is spectral blackbody radiance (Planck's law) at temperature T (assumed at 30°C):

$$\text{Specularity}\ (\lambda) = \frac{\rho_s(\lambda)}{\rho_s(\lambda)+\rho_d(\lambda)} \quad \text{(Equation 1)}$$

$$R_{solar} = \frac{\int_{0.3\mu m}^{2.5\mu m} I_{AM1.5G}(\lambda)[\rho_s(\lambda)+\rho_d(\lambda)]\ d\lambda}{\int_{0.3\mu m}^{2.5\mu m} I_{AM1.5G}(\lambda)\ d\lambda} \quad \text{(Equation 2)}$$

$$\varepsilon_{\lambda_1\ \text{to}\ \lambda_2}(T) = \frac{\int_{\lambda_1}^{\lambda_2} I_{bb}(\lambda,T)[1-\rho_s(\lambda)-\rho_d(\lambda)]\ d\lambda}{\int_{\lambda_1}^{\lambda_2} I_{bb}(\lambda,T)\ d\lambda} \quad \text{(Equation 3)}$$

Thermal measurements

Lab tests were performed with simulated sky, sun, and ground (Figure S8). An ice-water mixture placed in a plastic container (~27 × 47 cm) was used as the sky. A high-power lamp (Thorlabs HPLS-30-03) with an output light wavelength of 0.35–1 μm was used as the sun (zenith angle ~57°). A Rosco black cinefoil bought from Amazon.com was used as the ground, which has emissivity over 0.95 and specularity less than 0.1. The cinefoil (~31 × 93 cm) was heated by silicone heating pads under it, powered by a direct current voltage supply (Elenco XP-625). The sample was ~15 × 15 cm, assembled by reflectors, emitters, Al parts (McMaster-Carr 8982K54), substrate, K-type TCs (Omega 5TC-TT-K-30-72), and PS foam (McMaster-Carr 93475K63). The center of the sample was ~20 and ~15 cm away from the simulated sky and the ground, respectively, in the vertical direction. The TC readings were calibrated using a custom-made setup and were recorded using a data acquisition module (Measurement Computing USB-TC). See supplemental information section 2 for details.

Field tests were carried out on sunny days in August 2022 in a parking lot in Sparta Township, New Jersey (41°03′18.0″N, 74°37′21.3″W). The samples and controls were mounted on a cardboard box (~102 × 41 × 36 cm, exposed to air), and the box was covered with Al foil to remain cool under sunlight (Figure S12A). The box faced south, where only ~20° of its view from the horizon was blocked by trees (Figure S12B). A TC was placed inside the box and surrounded by white foam to measure the temperature of ambient air (Figure S12B). A TC was affixed on the ground to measure its temperature (Figure 3G). A pyranometer (Apogee SP-510) facing south was used to measure solar irradiance (Figure S12C). The temperatures of the samples were measured. The relative cooling power was estimated from the temperature data in Figure 3H (see supplemental information, section 3), and different conditions were explored to show our design's universal cooling effect. See supplemental information section 3 for details.

DATA AND CODE AVAILABILITY

All data are available in the manuscript or the supplemental information. Correspondence and requests for materials should be addressed to the lead contact, Y.Y.

SUPPLEMENTAL INFORMATION

Supplemental information can be found online at https://doi.org/10.1016/j.ynexs.2024.100028.

ACKNOWLEDGMENTS

We thank Sparta High School (Sparta Township, NJ) for providing the site to carry out the field tests. Y.Y. acknowledges support from the National Science Foundation (award no. 2005747) and the Urban Tech Award from Columbia University. J.M. acknowledges support from Schmidt Science Fellows, in partnership with the Rhodes Trust, and Princeton University faculty startup fund.

AUTHOR CONTRIBUTIONS

Y.Y., J.M., A.P.R., and Q.C. conceived the idea independently. Q.C. performed the simulations, prepared the samples, and conducted the experiments. S.G., G.H., and J.E.B. helped with sample preparation, lab tests, and field tests. A.A. and P.Z. helped with the EnergyPlus simulations. Y.X. helped with reflectance measurements. Y.Y., N.Y., and A.P.R. supervised the project. All authors contributed to the writing of the paper.

DECLARATION OF INTERESTS

The authors declare no competing interests.

Received: April 22, 2024
Revised: July 8, 2024
Accepted: July 10, 2024
Published Online: August 9, 2024

REFERENCES

1. U.S. Energy Information Administration (2022). Monthly Energy Review: October 2022. https://www.eia.gov/totalenergy/data/monthly/previous.php.
2. International Energy Agency (2018). The Future of Cooling. https://www.iea.org/reports/the-future-of-cooling.
3. Rephaeli, E., Raman, A., and Fan, S. (2013). Ultrabroadband Photonic Structures To Achieve High-Performance Daytime Radiative Cooling. Nano Lett. 13, 1457-1461.
4. Raman, A.P., Anoma, M.A., Zhu, L., et al. (2014). Passive radiative cooling below ambient air temperature under direct sunlight. Nature 515, 540-544.
5. Mandal, J., Fu, Y., Overvig, A.C., et al. (2018). Hierarchically porous polymer coatings for highly efficient passive daytime radiative cooling. Science 362, 315-319.
6. Li, D., Liu, X., Li, W., et al. (2021). Scalable and hierarchically designed polymer film as a selective thermal emitter for high-performance all-day radiative cooling. Nat. Nanotechnol. 16, 153-158.
7. Li, J., Liang, Y., Li, W., et al. (2022). Protecting ice from melting under sunlight via radiative cooling. Sci. Adv. 8, eabj9756. https://doi.org/10.1126/sciadv.abj9756.
8. Wang, L., Bai, G., Xue, P., et al. (2023). Ion Substitution Strategy toward Spectral Tunability of Environmentally Friendly Rare Earth Sulfide Lattices for Radiative Cooling. ACS Sustain. Chem. Eng. 11, 14236-14245.
9. Hossain, M.M., Jia, B., and Gu, M. (2015). A Metamaterial Emitter for Highly Efficient Radiative Cooling. Adv. Opt. Mater. 3, 1047-1051.
10. Zhai, Y., Ma, Y., David, S.N., et al. (2017). Scalable-manufactured randomized glass-polymer hybrid metamaterial for daytime radiative cooling. Science 355, 1062-1066.
11. Li, T., Zhai, Y., He, S., et al. (2019). A radiative cooling structural material. Science 364, 760-763.
12. Tian, Y., Shao, H., Liu, X., et al. (2021). Superhydrophobic and Recyclable Cellulose-Fiber-Based Composites for High-Efficiency Passive Radiative Cooling. ACS Appl. Mater. Interfaces 13, 22521-22530.
13. Zhou, K., Li, W., Patel, B.B., et al. (2021). Three-Dimensional Printable Nanoporous Polymer Matrix Composites for Daytime Radiative Cooling. Nano Lett. 21, 1493-1499.
14. Yao, P., Chen, Z., Liu, T., et al. (2022). Spider-Silk-Inspired Nanocomposite Polymers for Durable Daytime Radiative Cooling. Adv. Mater. 34, e2208236.
15. Tan, R., Hu, W., Yao, X., et al. (2024). Flexible and multifunctional composite films based on rare earth phosphors as broadband thermal emitters for high-performance passive radiative cooling. J. Mater. Chem. C Mater. 12, 2629-2638.
16. Tang, K., Dong, K., Li, J., et al. (2021). Temperature-adaptive radiative coating for all-season household thermal regulation. Science 374, 1504-1509.
17. Levinson, R., Berdahl, P., Akbari, H., et al. (2007). Methods of creating solar-reflective nonwhite surfaces and their application to residential roofing materials. Sol. Energy Mater. Sol. Cell. 91, 304-314.
18. Wang, S., Zhou, Y., Jiang, T., et al. (2021). Thermochromic smart windows with highly regulated radiative cooling and solar transmission. Nano Energy 89, 106440. https://doi.org/10.1016/j.nanoen.2021.106440.

19. Wang, S., Jiang, T., Meng, Y., et al. (2021). Scalable thermochromic smart windows with passive radiative cooling regulation. Science 374, 1501-1504.

20. Goldstein, E.A., Raman, A.P., and Fan, S. (2017). Sub-ambient non-evaporative fluid cooling with the sky. Nat. Energy 2, 17143. https://doi.org/10.1038/nenergy.2017.143.

21. Zhao, D., Aili, A., Zhai, Y., et al. (2019). Subambient Cooling of Water: Toward Real-World Applications of Daytime Radiative Cooling. Joule 3, 111-123.

22. Zou, H., Wang, C., Yu, J., et al. (2023). Eliminating greenhouse heat stress with transparent radiative cooling film. Cell Rep. Phys. Sci. 4, 101539.

23. Kallas, B. (1966). Asphalt pavement temperatures. Highw. Res. Rec. 1-11. https://trid.trb.org/View/100831.

24. Mohajerani, A., Bakaric, J., and Jeffrey-Bailey, T. (2017). The urban heat island effect, its causes, and mitigation, with reference to the thermal properties of asphalt concrete. J. Environ. Manage. 197, 522-538.

25. Albatici, R., Passerini, F., Tonelli, A.M., et al. (2013). Assessment of the thermal emissivity value of building materials using an infrared thermovision technique emissometer. Energy Build. 66, 33-40.

26. Mandal, J., Mandal, S., Brewer, J., et al. (2020). Radiative cooling and thermoregulation in the earth's glow. Preprint at arXiv. https://arxiv.org/abs/2006.11931.

27. Peng, Y.C., Fan, L.L., Jin, W.L., et al. (2021). Coloured low-emissivity films for building envelopes for year-round energy savings. Nat. Sustain. 5, 339-347.

28. Zhou, J., Chen, T.G., Tsurimaki, Y., et al. (2023). Angle-selective thermal emitter for directional radiative cooling and heating. Joule 7, 2830-2844.

29. Granqvist, C.G., and Hjortsberg, A. (1981). Radiative cooling to low temperatures: General considerations and application to selectively emitting SiO films. J. Appl. Phys. 52, 4205-4220.

30. Zhou, L., Song, H., Liang, J., et al. (2019). A polydimethylsiloxane-coated metal structure for all-day radiative cooling. Nat. Sustain. 2, 718-724.

31. Deru, M., Field, K., Studer, D., et al. (2011). US Department of Energy commercial reference building models of the national building stock. https://digitalscholarship.unlv.edu/renew_pubs/44/.

32. International Energy Conservation Code (2012). IECC Climate Zone Map. https://basc.pnnl.gov/images/iecc-climate-zone-map.

33. Corrugated Steel Sheets Market: Global Industry Analysis and Forecast (2023-2029). Retrieved from https://www.maximizemarketresearch.com/market-report/global-corrugated-steel-sheets-market/100759/. (2023).

34. Zheng, S., Li, C., Fu, Q., et al. (2016). Development of stable superhydrophobic coatings on aluminum surface for corrosion-resistant, self-cleaning, and anti-icing applications. Mater. Des. 93, 261-270.

35. Lei, M.-Q., Hu, Y.-F., Song, Y.-N., et al. (2021). Transparent radiative cooling films containing poly(methylmethacrylate), silica, and silver. Opt. Mater. 122, 111651. https://doi.org/10.1016/j.optmat.2021.111651.

36. Arrés Chillón, J., Paulillo, B., Mazumder, P., et al. (2022). Transparent Glass Surfaces with Silica Nanopillars for Radiative Cooling. ACS Appl. Nano Mater. 5, 17606-17612.

37. Zhou, K., Yan, X., Oh, S.J., et al. (2023). Hierarchically Patterned Self-Cleaning Polymer Composites for Daytime Radiative Cooling. Nano Lett. 23, 3669-3677.

38. Chen, G., Wang, Y., Qiu, J., et al. (2021). A visibly transparent radiative cooling film with self-cleaning function produced by solution processing. J. Mater. Sci. Technol. 90, 76-84.